Analysis of Metallic Waveguides with Rectangular Boundaries by Using the Finite-Difference Method and the Simultaneous Iteration with the Chebyshev Acceleration

Jenn-Ming Guan and Ching-Chuan Su, *Member, IEEE*

Abstract—**A numerical procedure based on the finite-difference method and simultaneous iteration of the power method in conjunction with the Chebyshev acceleration technique is utilized to analyze the metallic waveguides. Due to the efficiency of the present sparse matrix eigenproblem solver, lots of unknowns can be used in the domains of the waveguide cross-sections. Therefore, accurate cutoff wavenumbers or frequencies can be obtained by using the simple finite-difference method for the commonly used metallic waveguides such as the L-shaped, single-ridged, double-ridged, and rectangular coaxial waveguides. Some discrepancies with the numerical results in the recent literature are found and detailed discussions are provided to verify the correctness of the present results.**

I. Introduction

THE rectangular hollow metallic waveguide and many of its variations, such as the ridged waveguides [1], [2] for wider bandwidth operations are commonly used in microwave systems. More recently, the square corner cut rectangular waveguide (SCCRW), which is a special case of the L-shaped waveguides, is used by Liang *et al.* for the construction of the dual-mode filters for satellite communication [3]. The four-pole elliptic bandpass filter, which was realized at C-band, is composed of two sections of shorted SCCRW's coupled by one evanescent rectangular waveguide. The merit is that the SCCRW filter can be designed without any tuning mechanism. On the other hand, the rectangular coaxial waveguide constructed by a conducting strip shielded with metallic walls is also used as a transmission line [4], [5] or as a TEM cell [6] for electromagnetic compatibility. Recently, a linearly tapered TEM cell by the name of the GTEM cell is proposed by Leo *et al.* [7]. For the investigations of propagation characteristics along the GTEM cell [7] and scattering analysis when objects appear in the cells, the complete set of the waveguide modes of TEM cell (i.e., local waveguide modes of GTEM cell) are needed by the approaches using the eigenfunction expansions.

Most research on the related topics has been performed and collected in an early publication [8]. More recently, researches using the surface integral equation methods [9]–[12], the finite-element methods [13]–[16], and the finite-difference method [17] can be found. In the methods using the surface integral equation, the Galerkin procedure and the dyadic Green's function for the two-dimensional circular or rectangular cavity resonator are used in [9], [10]. While, the free-space Green's function and the method of moments with different expansion and testing functions are employed via the electric field [11] or magnetic field [12] formulation. The matrix dimension of the former formulation is less than that of the latter. However, the Green's function of the former is more complicated than that of the latter. As to the finite-element method, the Hermitian element with mesh refinement in the vicinity of the sharp metal edge [13] or the singular element at the sharp edge [14] has been applied via a formulation based on one longitudinal field component (E_z or H_z). On the other hand, the full $\boldsymbol{H}$ formulation is employed with the singular testing function [15] or the edge element [16] to treat the singularity of transverse fields at the sharp edge. The finite-element methods result in large and sparse matrix eigenvalue problems. In order to find the dominant eigenpairs accurately and efficiently, specific algorithms are needed as those have been employed in the finite-difference method discussed in the following.

The finite-difference methods have been utilized to treat the metallic waveguides by Beaubien and Wexler [18] and Sarkar *et al.* [17] with the corresponding matrix eigenproblems being solved by the successive over-relaxation (SOR) and conjugate gradient methods (CGM), respectively. With the criterion of high accuracy, large number of unknowns should be used to discretize the waveguide cross-section. However, due to the possible limited efficiency of the two above-mentioned algorithms for matrix eigenvalue problems, the reported results may not be accurate enough without using much finer grids. In this investigation, we employ the more efficient simultaneous iteration of the power method in conjunction with the Chebyshev acceleration technique to solve the large and sparse matrix eigenproblems resulting from applying the finite-difference method to the governing equations of metallic waveguides. The same approach has been successfully applied to the problem of dielectric-loaded cavities [19], [20]. In this investigation, we apply this method to the metallic waveguides problem. In Section II, this method is briefly described. In Section III, the numerical results are compared to the published

Manuscript received December 6, 1993; revised April 26, 1994.

The authors are with the Department of Electrical Engineering, National Tsinghua University, Hsinchu, Taiwan.

IEEE Log Number 9407290.

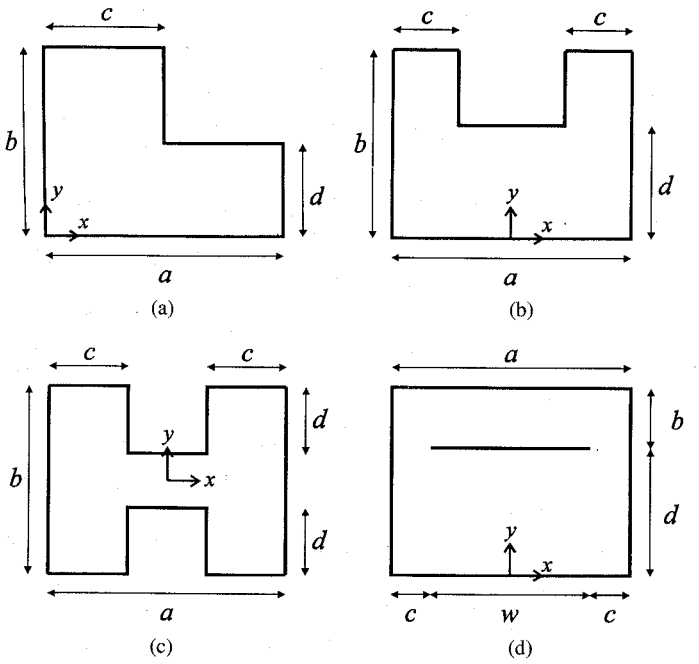

Fig. 1. Cross-sections of (a) L-shaped, (b) single-ridged, (c) double-ridged, and (d) rectangular coaxial waveguides.

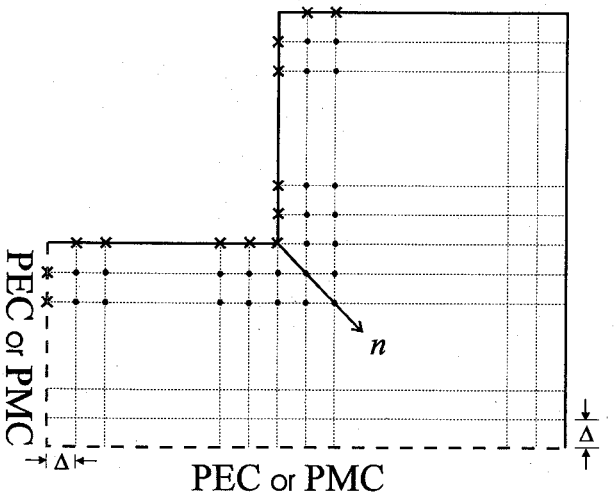

Fig. 2. Finite-difference grid and the normal direction at the nonconvex conductor edge. • • •: interior node points; × × ×: boundary node points

data in the literature to show the efficiency and accuracy of the present approach.

II. Formulation and Algorithm

The cross-sections of various metallic waveguides to be analyzed are shown in Fig. 1(a)–(d) for the L-shaped, single-ridged, double-ridged, and rectangular coaxial waveguides, respectively. The metallic outer or inner boundaries of the waveguides are assumed to be perfect electric conductors (PEC) and a strip conductor of zero thickness is assumed in the rectangular coaxial waveguide. At the nonconvex corner edges, a curvature of electrically small radius is defined there as done for the dielectric edge [20]. Hence, as shown in Fig. 2, the normal directions at these edge points are the vectors that bisect the angles between the two metallic walls [15].

It is well known that the propagation characteristics of the metallic waveguides with homogeneous permittivity and permeability distributions can be fully determined by the longitudinal component of electric or magnetic field Ψ as

$$\left(\frac{\partial^2}{\partial x^2}+\frac{\partial^2}{\partial y^2}+{k_c}^2\right)\Psi(x,\,y)=0, \tag{1}$$

where k_c is the cutoff wavenumbers. The corresponding boundary conditions are the Dirichlet and Neumann conditions at metallic boundary for the guiding TM and TE modes, respectively. By the symmetry of structures, only one half (Fig. 1(b) and (d)) or one quarter (Fig. 1(c) and (d) with $b=d$) of the cross-section should be considered for some waveguides with the PEC or PMC (perfect magnetic conductor) conditions in the symmetry planes. By the use of the equally spaced five-point finite-difference formula, (1) becomes the simultaneous algebraic equations

$$\Psi_{i+1,j}+\Psi_{i-1,j}+\Psi_{i,j+1}+\Psi_{i,j-1}-4\Psi_{ij}=-(k_c\Delta)^2\Psi_{ij}, \tag{2}$$

where $\Psi_{ij}=\Psi(i\Delta,\,j\Delta)$ for all the interior node points and Δ is the size of the square meshes in the finite-difference grid as shown in Fig. 2. It is noted that the equally-spaced grid points coincide with the metallic boundaries. In (2), the nodal fields at the metallic walls and symmetry planes are either zero or evaluated in terms of neighboring nodal fields via the Neumann condition for which the three-point forward or backward difference is used.

A standard eigenvalue problem $\mathbf{Ax}=\lambda\mathbf{x}$ is obtained from (2) with eigenvalue $\lambda=-(k_c\Delta)^2$. The real matrix $\mathbf{A}$ is symmetric only when all the boundaries of considered region have the Dirichlet condition. The eigenvalues of matrix $\mathbf{A}$ are located between -8 and zero from Gerschgorin's theorem. The desired eigenvalues are the least-magnitude ones that correspond to the cutoff wavenumbers of the dominant modes of waveguides by the relation $k_c=\sqrt{|\lambda|}/\Delta$. When finer grids are used for high accuracy, the dimension of matrix $\mathbf{A}$ will become very large and the eigenvalues will closely cluster. As a result, the Chebyshev acceleration technique is needed to accelerate the convergence rate of the simultaneous iteration of the power method for obtaining the eigenpairs of matrix $\mathbf{A}$ corresponding to dominant modes.

The simultaneous iteration with the Chebyshev acceleration (SIC) is fully discussed in [20] and [21]. The method is briefly described here. For obtaining q desired eigenpairs of matrix $\mathbf{A}$ of order M with p $(\geq q)$ iteration vectors and preconditioning by the Chebyshev polynomial of degree n denoted by $T_n(x)$, matrix $\mathbf{A}$ is scaled to matrix $\mathbf{B}$ as

$$\mathbf{B}=\frac{2}{c_2-c_1}\left\{\mathbf{A}-\frac{c_1+c_2}{2}\mathbf{I}\right\}, \tag{3}$$

where $c_1=-8$; c_2 is a small negative number that corresponds to the maximum cutoff wavenumber that can be calculated; and $\mathbf{I}$ is a unity matrix of order M. Thereafter, the numerical procedures consist of the following six steps:

1) Start with p linearly independent vectors

$$\mathbf{X}_0 = [\mathbf{x}_1, \cdots, \mathbf{x}_p];$$

2) Compute matrix-vector multiplications

$$T_n(\mathbf{B})\mathbf{X}_k; \qquad k = 0, 1, 2, \cdots$$

3) Find $p \times p$ matrices $\mathbf{C}_k$ and $\mathbf{\Lambda}_k$ $(= \text{diag}[\gamma_1, \gamma_2, \cdots, \gamma_p])$ corresponding to the eigenpairs of the transformed problem

$$(\mathbf{X}_k{}^{\mathrm{T}} T_n(\mathbf{B})\mathbf{X}_k)\mathbf{C}_k = (\mathbf{X}_k{}^{\mathrm{T}}\mathbf{X}_k)\mathbf{C}_k\mathbf{\Lambda}_k; \qquad (4)$$

4) Form new vectors : $\mathbf{X}_{k+1} = (T_n(\mathbf{B})\mathbf{X}_k)\mathbf{C}_k$ and normalize each vector of $\mathbf{X}_{k+1}$
5) Take Rayleigh quotients to obtain eigenvalues λ_i of matrix $\mathbf{A}$

$$\lambda_i = \frac{(\mathbf{x}_i, \mathbf{A}\mathbf{x}_i)}{(\mathbf{x}_i, \mathbf{x}_i)}; \qquad i = 1, 2, \cdots, q \qquad (5)$$

6) Make convergence test and go to step 2 if not converged.

Most of the computation time is to evaluate the matrix-vector multiplications in step 2. The number of multiplication operation for two real-typed variables is $2 \times n \times p \times M$ for step 2 in each cycle.

III. Numerical Results

The metallic waveguides with rectangular boundaries shown in Fig. 1 are analyzed in the following subsections with the examples investigated in the recent literature. The cutoff wavenumbers or frequencies and eigenfield distributions of the TE or TM modes are presented in the corresponding tables and figures. In treating the TE modes of the L-shaped waveguide and the rectangular coaxial waveguide with off-centered strip (Table V) or the symmetric TE modes of the single-ridged waveguide, there is a null mode with the eigenvalue being equal to zero and all the components of the corresponding eigenvector being equal to one constant due to the Neumann conditions in all the boundaries. This null mode appears first in applying the finite-difference method and simultaneous iteration with the Chebyshev acceleration (FD-SIC). However, this null mode does not exist physically and is removed from the corresponding tables.

A. Double-ridged Waveguide

The first example that will be analyzed is the double-ridged waveguide depicted in Fig. 1(c) with $a = 1.27$ cm, $b = 1.016$ cm, $c = 0.508$ cm, and $d = 0.3683$ cm, which has been analyzed by other approaches [1], [2], [13], [14], [16]. By utilizing symmetry in the x and y directions, two grids of 50 by 40 and 100 by 80 are used to fit the metallic boundaries exactly for one quarter of the waveguide cross-section. The calculated cutoff wavenumbers for the y-antisymmetric (odd function of y) TE modes are shown in Table I together with the results by other approaches. It is noted that the symmetry type is referred to field H_z for TE modes and to field E_z for TM modes through this investigation. The $TE_{10}H$, $TE_{20}T$, and $TE_{30}H$ modes are the first three x-symmetric (even function of x) modes, while the $TE_{10}T$ and $TE_{11}T$ modes are the first two x-antisymmetric modes. It is seen that our FD-SIC results for both grids are in good agreement with those in the literature except for the $TE_{10}H$ mode with the 50 by 40 grid. Because the lower-order modes are much more dominant at the conductor edge, dense grids should be used in the vicinity of the edge for the $TE_{10}H$ mode as shown by the result of the 100 by 80 grid. The required number of iterations, for example, for the first three x-symmetric modes to converge to the fourth decimal is about 800 for the 100 by 80 grid with $p = q = 3$, $n = 50$, and $c_2 = -1.1 \times 10^{-3}$, which corresponds to the upper limit of the calculated cutoff wavenumber being 10 rad/cm. The corresponding computation time is about 3 min on a 486DX-33 personal computer with the compiler of the Microsoft Fortran Powerstation.

TABLE I
Comparison of the Cutoff Wavenumbers k_c (rad/cm) for the Double-Ridged Waveguide ($a = 1.27$ cm $b = 1.016$ cm, $c = 0.508$ cm, $d = 0.3683$ cm)

Mode	$TE_{10}H$	$TE_{10}T$	$TE_{20}T$	$TE_{30}H$	$TE_{11}T$
FD-SIC 50×40	1.428	3.169	6.192	6.695	6.976
FD-SIC 100×80	1.434	3.168	6.192	6.705	6.975
Montgomery [1]	1.437	3.166	6.190	6.712	6.973
Utsumi [2]	1.438	3.155	6.215	6.707	6.971
scalar-FEM [13]	1.440	—	6.192	6.713	—
singular-FEM [14]	1.439	—	6.193	6.714	—
vector-FEM [16]	1.137	—	6.197	6.721	—

B. L-shaped and Single-ridged Waveguides

The next examples are the L-shaped waveguide with $a = b = 1.27$ cm and $c = d = a/2$, depicted in Fig. 1(a), and the single-ridged waveguide with $a = 1.0$ cm, $b = 0.5$ cm, and $c = d = 0.25$ cm, depicted in Fig. 1(b). By the use of symmetry of the single-ridged waveguide, only one half of the domain is considered and the eigenproblems for the antisymmetric (A) TM modes and symmetric (S) TE modes are equivalent to those of the L-shaped waveguide for the TM and TE modes, respectively. The associated eigenvalues are identical with the same discretization in the considered domain of the waveguide cross-sections, and the corresponding cutoff wavenumbers can be obtained by scaling the dimensions of the structures. That is, the cutoff wavenumbers are inversely proportional to the dimension b, c, or d of the considered L-shaped and single-ridged waveguides for the corresponding modes. A 50 by 50 grid is used to calculate a few dominant cutoff wavenumbers of the TM and TE modes for the two waveguides. The numerical results are shown in Tables II and III for the L-shaped and single-ridged waveguides, respectively. The mode designation used in this investigation for the L-shaped and single-ridged waveguides is that the TE and TM modes are followed by an integer subscript in ascending order of the cutoff wavenumbers. The degenerate modes are also counted. Also shown in the Tables are the results of the surface integral equation (SIE) method [11] and the finite-difference with conjugate gradient method (FD-CGM) [17] by

TABLE II
COMPARISON OF THE CUTOFF WAVENUMBERS k_c (RAD/CM) FOR THE L-SHAPED WAVEGUIDE. ($a = b = 1.27$ CM, $c = d = a/2$)

Mode	SIE [11]	FD-CGM [17]	Present FD-SIC	Analytic Solution	Differences between FD-SIC and SIE	FD-CGM	Analytic
TM_1	4.8677	4.80	4.8949	—	0.56 %	1.98 %	—
TM_2	6.1361	6.07	6.1350	—	0.02 %	1.07 %	—
TM_3	6.9908	6.92	6.9921	6.9967	0.02 %	1.04 %	0.07 %
TM_4	8.5525	8.61	8.5458	—	0.08 %	0.75 %	—
TM_5	—	9.72	8.8940	—	—	9.28 %	—
TM_6	—	11.39	10.1262	—	—	12.48 %	—
TM_7	—	—	10.5318	—	—	—	—
TM_8	—	—	11.0380	11.0627	—	—	0.22 %
TM_9	—	—	11.0380	11.0627	—	—	0.22 %
TM_{10}	—	—	11.8407	—	—	—	—
TE_1	1.8917	1.88†	1.9111	—	1.02 %	1.65 %	—
TE_2	2.9159	2.95†	2.9600	—	1.51 %	0.34 %	—
TE_3	4.8755	4.89†	4.9452	4.9474	1.43 %	1.13 %	0.04 %
TE_4	—	—	4.9452	4.9474	—	—	0.04 %
TE_5	5.2463	5.26†	5.3128	—	1.27 %	1.00 %	—
TE_6	—	5.49†	5.5799	—	—	1.64 %	—
TE_7	—	6.91†	6.9937	6.9967	—	1.21 %	0.04 %
TE_8	—	—	7.2784	—	—	—	—
TE_9	—	—	7.6002	—	—	—	—

converting their dimensionless or normalized quantities. It is noted that the cutoff wavenumbers of the TE modes by the FD-CGM in Table II are indicated for dimensionless $a = 1.3$ [Table 8, 17]. However, the result for TE_1 mode in [17] is compared by the same group of researchers to those by the SIE method for dimensionless $a = 1.27$ [11]. Hence, these data are assumed for $a = 1.27$ cm in this investigation; otherwise, the discrepancies are severer.

From Tables II and III it is seen that for some modes the results by the SIE are very close to the present solutions but for the other modes discrepancies of 1 to 2 % are found. As to the FD-CGM, most of their results are smaller than our results and the discrepancies between the two methods are about 1%–2%. However, there are some significant discrepancies between the FD-CGM results and the present solutions. First, the calculated cutoff wavenumbers of TM_5 and TM_6 modes of the L-shaped waveguide by the FD-CGM are not close to any of our results for the modes from TM_5 to TM_{10}. Secondly, the cutoff wavenumber of TM_6 mode of the single-ridged waveguide does not appear by the FD-CGM.

By using the corresponding equivalence of eigenvalue problems between the L-shaped and the single-ridged waveguides, the cutoff wavenumber for the TM_6 mode of the single-ridged waveguide should be 17.58 ($6.92 \times 1.27/0.5$) rad/cm by the FD-CGM result for the TM_3 mode of the L-shaped waveguide. Hence, it is evident that the TM_6 mode in Table III is lost in the FD-CGM computation for the single-ridged waveguide. In addition, one may check the consistency between the results of the two waveguides by the individual method. It is found that there exists inconsistency of 2–3% for the TE modes in the solutions by the SIE method (the TE_1 and TE_2 modes of the L-shaped waveguide versus the TE_2 and TE_4 modes of the single-ridged waveguide, respectively). Furthermore, it is examined by the present approach that the cutoff wavenumbers (i.e. eigenvalues) of the TM_8 and TE_3 modes of the L-shaped waveguide, and hence the TE_6 mode of the single-ridged waveguide are with double degeneracy as shown in Tables II and III. However, these phenomena were not mentioned in the previous publications [11], [17]. Evidence of the degeneracy is provided in the following paragraph.

The L-shaped waveguide considered in this investigation occupies the space of three quarters of the square waveguide of width a. By the symmetry of the extended square waveguide, the PEC or PMC condition can be imposed at the two middle section planes, which coincide with part of the boundary of the L-shaped waveguide considered in this investigation, to obtain the guided modes of the square waveguide. Thus, the L-shaped waveguide considered in this investigation has the modes corresponding to those of the extended waveguide with the PEC condition at the two middle section planes of the extended waveguide. The eigenfield distributions of the L-shaped waveguide for field E_z of some TM modes and field H_z of some TE modes are illustrated in Figs. 3 and 4, respectively. As seen quantitatively from the computed cutoff wavenumbers and qualitatively from the eigenfields, the TM_3, (TM_8, TM_9), (TE_3, TE_4), and TE_7 modes are corresponding to the TM^{22}, (TM^{24}, TM^{42}), (TE^{02}, TE^{20}), and TE^{22} modes, respectively, of the extended waveguide, where the parenthesized modes are degenerate. Note that integer superscripts are employed for the commonly used mode designation of the rectangular waveguide in this investigation to avoid confusion with the present mode designation. Therefore, exact analytic solutions exist for these modes and the relative differences between our results and these analytic answers are shown in Table II to

TABLE III
COMPARISON OF THE CUTOFF WAVENUMBERS k_c (RAD/CM) FOR THE SINGLE-RIDGED WAVEGUIDE ($a = 1.0$ CM, $b = 0.5$ CM, $c = d = 0.25$ CM)

Mode	Type	SIE [11]	FD-CGM [17]	Present FD-SIC	Difference (FD-SIC & SIE)	Difference (FD-SIC & [17])
TM_1	S	12.0381	12.05	12.1447	0.90 %	0.79 %
TM_2	A	12.2938	12.32	12.4331	1.16 %	0.92 %
TM_3	S	13.9964	13.86	14.0037	0.03 %	1.04 %
TM_4	A	15.5871	15.34	15.5829	0.06 %	1.58 %
TM_5	S	—	16.28	16.6403	—	2.21 %
TM_6	A	—	—	17.7598	—	—
TM_7	S	—	19.32	19.6296	—	1.60 %
TM_8	A	—	—	21.7063	—	—
TE_1	A	2.2496	2.23	2.2422	0.33 %	0.55 %
TE_2	S	4.9436	4.78	4.8543	1.81 %	1.55 %
TE_3	A	6.5189	6.40	6.4476	1.09 %	0.74 %
TE_4	S	7.5642	7.48	7.5185	0.60 %	0.51 %
TE_5	A	—	9.71	9.8314	—	1.25 %
TE_6	S	—	12.39	12.5607	—	1.38 %
TE_7	S	—	—	12.5607	—	—
TE_8	A	—	—	12.7667	—	—
TE_9	A	—	—	13.3825	—	—

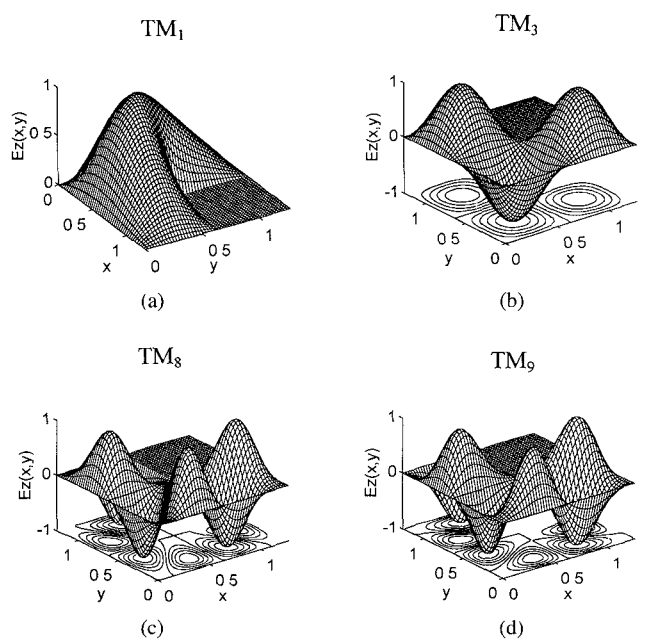

Fig. 3. Field E_z distributions of the (a) TM_1, (b) TM_3, (c) TM_8, and (d) TE_9 modes for the L-shaped waveguide considered in Table II.

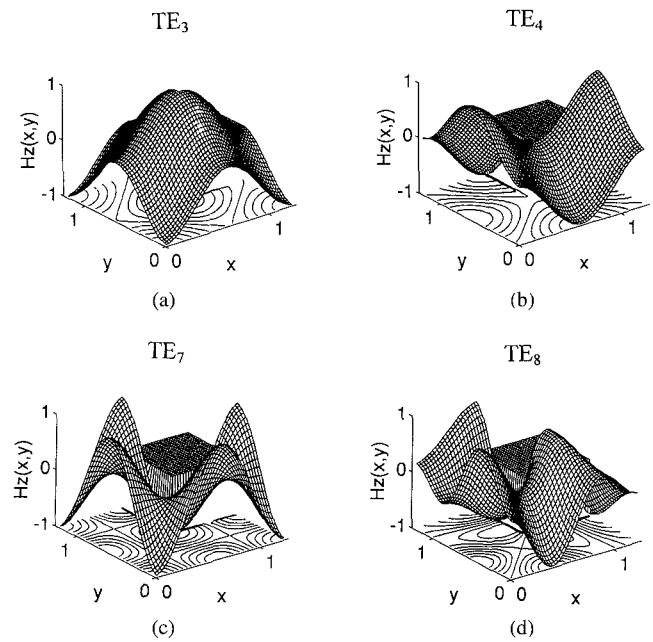

Fig. 4. Field H_z distributions of the (a) TE_3, (b) TE_4, (c) TE_7, and (d) TE_8 modes for the L-shaped waveguide considered in Table II.

demonstrate the accuracy of the present FD-SIC method. The calculated field distributions of the two degenerate TM_8 and TM_9 modes shown in Fig. 3(c) and (d) are two different linear combinations of the eigenfields of the two degenerate TM^{24} and TM^{42} modes of the extended square waveguide. The same situation holds for the dual TE_3 and TE_4 modes corresponding to the TE^{02} and TE^{20} modes as shown in Fig. 4(a) and (b).

C. Rectangular Coaxial Waveguides

The rectangular coaxial waveguides or the shielded striplines considered are the two examples analyzed in [7] for the GTEM cells by the transverse resonance diffraction (TRD) method. The first example bears symmetry in both x and y directions with $a = 6$ m, $b = d = 3$ m, and $w = 5$ m. The second example bears symmetry only in x direction with $a = 6$ m, $b = 1$ m, $d = 3$ m, and $w = 5$ m. Only the results of the TE modes are presented in [7] and this investigation. Furthermore, the y-symmetric modes of the first shielded stripline that can be solved analytically are also excluded from [7] and this investigation. To avoid the field allocation at the edge point of the strip, a 123 by 123 grid and a 123 by 164 grid are used for one quarter of the cross-section of the first stripline and for one half of the cross-section of the

TABLE IV
COMPARISON OF THE CUTOFF FREQUENCIES (MHz) FOR THE FIRST y-ANTISYMMETRIC SEVENTEEN DOMINANT TE MODES OF THE RECTANGULAR COAXIAL WAVEGUIDE ($a = 6$ M, $b = d = 3$ M, $w = 5$ M)

Mode	Type	TRD [7]	Present FDM	Difference (FDM & TRD)
TE_1	S	14.270	14.203	0.47 %
TE_3	A	31.819	31.786	0.10 %
TE_6	S	—	50.016	—
TE_8	S	57.374	57.351	0.04 %
TE_9	A	64.089	64.032	0.09 %
TE_{12}	A	—	78.171	—
TE_{13}	S	79.451	79.399	0.07 %
TE_{15}	A	94.558	94.605	0.05 %
TE_{18}	S	—	100.122	—
TE_{20}	S	103.453	103.486	0.03 %
TE_{21}	A	111.480	111.399	0.07 %
TE_{24}	S	—	111.930	—
TE_{27}	A	—	125.117	—
TE_{28}	S	125.244	125.175	0.06 %
TE_{29}	A	130.395	130.412	0.01 %
TE_{31}	A	139.974	140.039	0.05 %
TE_{33}	S	144.152	144.222	0.05 %

second stripline in the right-hand side, respectively. It is noted that the field H_z is discontinuous at the infinitely thin strip in general. That is, the fields $H_z(x,\ y = d^+)$ on the upper side of the strip may be different from those $H_z(x,\ y = d^-)$ on the lower side. Therefore, the fields $H_z(x,\ y = d^+)$ and $H_z(x,\ y = d^-)$ for $0 < x < \frac{w}{2}$ are evaluated with the forward and backward difference formulas, respectively, via the Neumann condition in the computation for the second stripline. In addition, the second partial derivative $\partial^2/\partial x^2$ for the point just to the right of the strip edge is substituted by the three-point forward difference formula.

The calculated results are shown in Tables IV and V for the first and second shielded striplines, respectively. The mode designation is the same as that for the L-shaped and single-ridged waveguides. Hence, the y-symmetric modes of the first stripline are also counted although they are not shown in Table IV. Also shown in the Tables are the results by the TRD method and their differences with the present approach. It is seen that these two results are in good agreement, especially for the high-order modes. However, our results contain some modes that did not appear in [7]. In what follows, we show that at least parts of them are indeed physical modes.

In Table IV there are five modes not appearing in [7]: the TE_6, TE_{12}, TE_{18}, TE_{24}, and TE_{27} modes. It is interesting to note that the cutoff frequencies of the y-antisymmetric TE_6, TE_{18}, TE_{24}, and TE_{27} modes in Table IV are very close to those of the y-symmetric and degenerate (TE_4, TE_5), (TE_{16}, TE_{17}), (TE_{22}, TE_{23}), and (TE_{25}, TE_{26}) modes, respectively. These four pair of dual y-symmetric modes are equivalent to the (TE^{02}, TE^{20}), (TE^{04}, TE^{40}), (TE^{24}, TE^{42}), and (TE^{34}, TE^{50}) modes, respectively, of the hollow square waveguide having the same dimension as the shielded stripline without the strip [22]. Hence, the cutoff frequencies of these dual modes are 50, 100, 111.803, and 125 MHz, respectively. The reason that the cutoff frequencies of these four y-antisymmetric modes are close to the corresponding dual modes can be explained by observing the eigenfield distributions. For example, the eigenfield H_z distributions of the TE_{22}, TE_{23}, and TE_{24} modes are shown in Figs. 5(a)–(c) for one quarter of the cross-section of the first stripline. By the linear combinations of the fields of Figs. 5(a) and 5(b) as

$$\frac{1}{2}(\cos\frac{\pi}{3}x\ \cos\frac{2\pi}{3}y + \cos\frac{2\pi}{3}x\ \cos\frac{\pi}{3}y), \tag{6a}$$

the resulting fields shown in Fig. 5(d) are very close to the fields of the TE_{24} mode except the regions near the strip edge. The boundary conditions of the (TE^{24}, TE^{42}) modes and those of the TE_{24} mode are identical except that from $x = 2.5$ m to $x = 3$ m ($y = 0$) where the Dirichlet condition is imposed for the TE_{24} mode. It is seen from Fig. 5(d) that the fields are approaching to zero (the Dirichlet condition) from $x = 2.5$ m to $x = 3$ m ($y = 0$). Thus, the actual fields of the TE_{24} mode are slightly perturbed from the fields of Fig. 5(d) in the vicinity of the strip edge. Owing to the similarity in field distributions, it can be expected that the cutoff frequency of the TE_{24} mode is close to that of the dual (TE_{22}, TE_{23}) modes. The same situations hold for the TE_6, TE_{18}, and TE_{27} modes corresponding to the (TE^{02}, TE^{20}), (TE^{04}, TE^{40}), and (TE^{34}, TE^{50}) modes, respectively. The field H_z distributions of the TE_6, TE_{18}, and TE_{27} modes shown in Fig. 6(a)–(c) resemble those of

$$-\frac{1}{2}(\cos\frac{\pi}{3}y + \cos\frac{\pi}{3}x), \tag{6b}$$

$$\frac{1}{2}(\cos\frac{2\pi}{3}y - \cos\frac{2\pi}{3}x), \tag{6c}$$

and

$$\frac{1}{2}(\sin\frac{\pi}{2}x\ \cos\frac{2\pi}{3}y + \sin\frac{5\pi}{6}x), \tag{6d}$$

respectively. The eigenfield of the remaining TE_{12} mode not appearing in [7] is shown in Fig. 6(d).

As to the second shielded stripline, there are ten modes that do not appear in [7] compared to the present FD-SIC results shown in Table V. If the electric field of a mode in a rectangular waveguide is only in the y direction, the presence of an infinitely thin conducting strip will have no effect on that mode. Thus, the TE^{10}, TE^{20}, TE^{30}, TE^{40}, and TE^{50} modes of the hollow rectangular waveguide having the same dimension as the shielded stripline without the strip are also modes of the shielded stripline. According to the calculated cutoff frequencies and eigenfields, partly shown in Fig. 7 for one half of the cross-section of the second stripline, the TE_2, TE_4, TE_8, TE_{12}, and TE_{18} modes, among the just-mentioned 10 modes missing in [7], correspond to the above five rectangular waveguide modes, respectively. The fields on the lower and upper sides of the strip are discontinuous in general. Thus, the location of the strip can be inferred from the discontinuity if it exists in Fig. 7. However, the fields on the strip are continuous for the just-mentioned five modes having the analytic solutions. The numerical deviations from the continuity of fields on the strip are more obvious in the

TABLE V
COMPARISON OF THE CUTOFF FREQUENCIES (MHZ) FOR THE FIRST TWENTY-TWO DOMINANT TE MODES OF THE RECTANGULAR COAXIAL WAVEGUIDE. (a = 6 M, b = 1 M, d = 3 M, w = 5 M)

Mode	Type	TRD [7]	Present FDM	Analytic Solution	Difference (FDM & TRD)	Difference (FDM & Analytic)
TE_1	S	19.980	19.887	—	0.47 %	—
TE_2	A	—	25.000	25	—	0.00 %
TE_3	A	38.611	38.530	—	0.21 %	—
TE_4	S	—	49.999	50	—	0.00 %
TE_5	S	—	50.013	—	—	—
TE_6	S	60.865	60.822	—	0.07 %	—
TE_7	A	61.069	61.027	—	0.07 %	—
TE_8	A	—	74.996	75	—	0.01 %
TE_9	S	77.215	77.151	—	0.08 %	—
TE_{10}	A	81.638	81.646	—	0.01 %	—
TE_{11}	A	93.925	93.956	—	0.03 %	—
TE_{12}	S	—	99.991	100	—	0.01 %
TE_{13}	S	—	100 113	—	—	—
TE_{14}	S	104.658	104.704	—	0.04 %	—
TE_{15}	A	107.864	107.822	—	0.04 %	—
TE_{16}	S	—	111.861	—	—	—
TE_{17}	S	119.582	119.576	—	0.01 %	—
TE_{18}	A	—	124.981	125	—	0.03 %
TE_{19}	A	—	125.140	—	—	—
TE_{20}	A	129.521	129.583	—	0.05 %	—
TE_{21}	A	—	136.650	—	—	—
TE_{22}	S	142.286	142.368	—	0.06 %	—

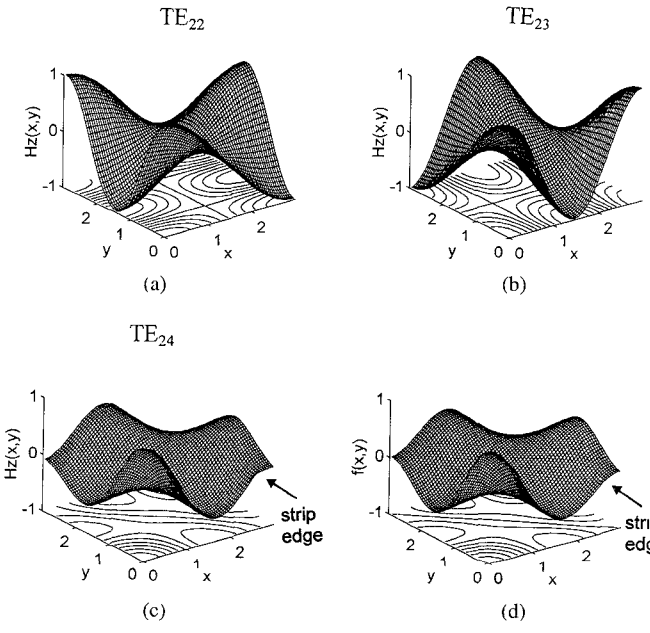

Fig. 5. Field H_z distributions of the (a) TE_{22}, (b) TE_{23}, and (c) TE_{24} modes for one quarter of the cross-section of the rectangular coaxial waveguide considered in Table IV. (d) $f(x, y) = \frac{1}{2}(\cos\frac{\pi}{3}x\ \cos\frac{2\pi}{3}y + \cos\frac{2\pi}{3}x\ \cos\frac{\pi}{3}y)$.

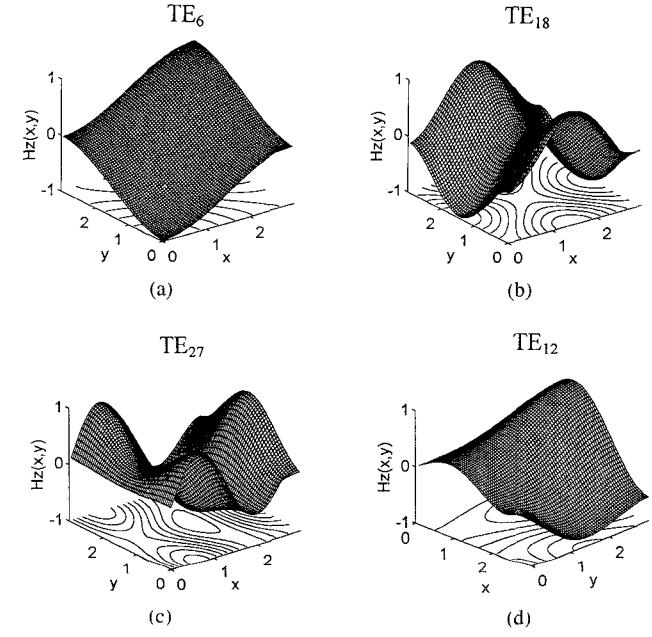

Fig. 6. Field H_z distributions of the (a) TE_6, (b) TE_{18}, (c) TE_{27}, and (d) TE_{12} modes for one quarter of the cross-section of the rectangular coaxial waveguide considered in Table IV.

TE_4 mode among these modes. The discontinuity errors are maximum near the center of the strip for the TE_4 mode and are about 1% there.

From the present FD-SIC results, the cutoff frequencies of the TE_5, TE_{13}, and TE_{19} modes are very close to those of the TE_4, TE_{12}, and TE_{18} modes, respectively. Hence, it may be difficult to find these nearly degenerate modes by the root-searching method used in the TRD method [7] if these modes can be solved by it. However, this situation does not cause any troubles for the present approach. At last, the field distributions of H_z for the remaining TE_{16} and TE_{21} modes not appearing in [7] are shown in Fig. 7(e) and (h), respectively.

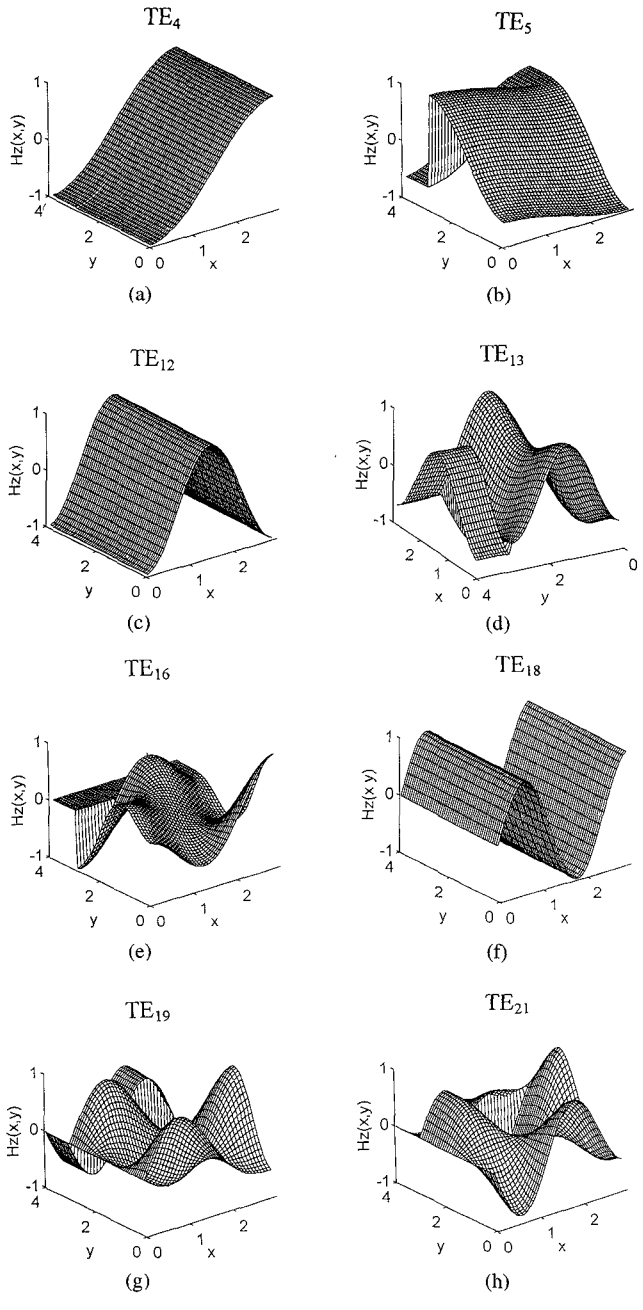

Fig. 7. Field H_z distributions of the (a) TE_4, (b) TE_5, (c) TE_{12}, (d) TE_{13}, (e) TE_{16}, (f) TE_{18}, (g) TE_{19}, and (h) TE_{21} modes for one half of the cross-section of the rectangular coaxial waveguide considered in Table V. The discontinuity is the location of the strip.

IV. Conclusion

The cutoff wavenumbers or frequencies of the TE or TM modes for the L-shaped, single-ridged, double-ridged, and rectangular coaxial waveguides are investigated in this paper by using the finite-difference method and the simultaneous iteration in conjunction with the Chebyshev acceleration technique. Accurate results are obtained by utilizing dense finite-difference grids and the efficient SIC algorithm for the sparse matrix eigenvalue problems. Although the problems of the metallic waveguides have been investigated for a long time, it is found that results of some modes in the recent literature are not satisfactory. Furthermore, it is found that a lot of modes are missing in recent publications. Detailed discussions and explanations have been provided to support our results.

References

[1] J. P. Montgomery, "On the complete eigenvalue solution of ridged waveguide," *IEEE Trans. Microwave Theory Tech.*, vol. MTT-19, pp. 547–555, June 1971.

[2] Y. Utsumi, "Variational analysis of ridged waveguide modes," *IEEE Trans. Microwave Theory Tech.*, vol. MTT-33, pp. 111–120, Feb. 1985.

[3] X.-P. Liang, K. A. Zaki, and A. E. Atia, "Dual mode coupling by square corner cut in resonators and filters," *IEEE Trans. Microwave Theory Tech.*, vol. MTT-40, pp. 2294–2302, Dec. 1992.

[4] J. C. Tippet and D. C. Chang, "Characteristic impedance of a rectangular coaxial line with offset inner conductor," *IEEE Trans. Microwave Theory Tech.*, vol. MTT-26, pp. 876–883, Nov. 1978.

[5] L. Gruner, "Characteristics of crossed rectangular coaxial structures," *IEEE Trans. Microwave Theory Tech.*, vol. MTT-28, pp. 622–627, June 1980.

[6] M. L. Crawford, "Generation of standard EM fields using TEM transmission cells," *IEEE Trans. Electromagn. Compat.*, vol. EMC-16, pp. 189–195, Nov. 1974.

[7] R. de Leo, T. Rozzi, C. Svara, and L. Zappelli, "Rigorous analysis of the GTEM cell," *IEEE Trans. Microwave Theory Tech.*, vol. MTT-39, pp. 488–500, Mar. 1991.

[8] F. L. Ng, "Tabulation of methods for the numerical solution of the hollow waveguide problem," *IEEE Trans. Microwave Theory Tech.*, vol. MTT-22, pp. 322–329, Mar. 1974.

[9] G. Conciauro, M. Bressan, and C. Zuffada, "Waveguide modes via an integral equation leading to a linear matrix eigenvalue problem," *IEEE Trans. Microwave Theory Tech.*, vol. MTT-32, pp. 1495–1504, Nov. 1984.

[10] L. Carbonini, "Modal analysis of multi-connected waveguides," *IEEE Trans. Microwave Theory Tech.*, vol. MTT-40, pp. 665–671, Apr. 1992.

[11] M. Swaminathan, E. Arvas, T. K. Sarkar, and A. R. Djordjević, "Computation of cutoff wavenumbers of TE and TM modes in waveguides of arbitrary cross sections using a surface integral formulation," *IEEE Trans. Microwave Theory Tech.*, vol. MTT-38, pp. 154–159, Feb. 1990. For comments, see MTT-38, pp. 1761–1762, Nov. 1990.

[12] W. Sun and C. A. Balanis, "MFIE analysis and design of ridged waveguides," *IEEE Trans. Microwave Theory Tech.*, vol. MTT-41, pp. 1965–1971, Nov. 1993.

[13] M. Israel and R. Miniowitz, "An efficient finite element method for nonconvex waveguide based on Hermitian polynomials," *IEEE Trans. Microwave Theory Tech.*, vol. MTT-35, pp. 1019–1026, Nov. 1987.

[14] J. M. Gil and J. Zapata, "Efficient singular element for finite element analysis of quasi-TEM transmission lines and waveguides with sharp metal edges," *IEEE Trans. Microwave Theory Tech.*, vol. MTT-42, pp. 92–98, Jan. 1994.

[15] J. P. Webb, "Finite element analysis of dispersion in waveguides with sharp metal edges," *IEEE Trans. Microwave Theory Tech.*, vol. MTT-36, pp. 1819–1824, Dec. 1988.

[16] R. Miniowitz and J. P. Webb, "Covariant-projection quadrilateral elements for the analysis of waveguides with sharp edges," *IEEE Trans. Microwave Theory Tech.*, vol. MTT-39, pp. 501–505, Mar. 1991.

[17] T. K. Sarkar, K. Athar, E. Arvas, M. Manela, and R. Lade, "Computation of the propagation characteristics of TE and TM modes in arbitrarily shaped hollow waveguides utilizing the conjugate gradient method," *J. Electromagn. Waves Appl.*, vol. 3, no. 2, pp. 143–165, 1989.

[18] M. J. Beaubien and A. Wexler, "Unequal-arm finite-difference operators in the positive-definite successive over-relaxation (PDSOR) algorithm," *IEEE Trans. Microwave Theory Tech.*, vol. MTT-18, pp. 1132–1149, Dec. 1970.

[19] C. C. Su and J. M. Guan, "Finite-difference analysis of dielectric-loaded cavities with the Chebyshev acceleration technique," in *Proc. 9th Conf. on the Computation of Electromagnetic Fields*, Miami, Oct. 1993, pp. 346–347.

[20] ——, "Finite-difference analysis of dielectric-loaded cavities using the simultaneous iteration of the power method with the Chebyshev acceleration technique," to appear in *IEEE Trans. Microwave Theory Tech.*

[21] Y. Saad, "Chebyshev acceleration techniques for solving nonsymmetric eigenvalue problems," *Math. Comp.*, vol. 42, pp. 567–588, Apr. 1984.

[22] L. Gruner, "Lower and upper bounds of cutoff frequencies in metallic waveguides," *IEEE Trans. Microwave Theory Tech.*, vol. MTT-40, pp. 995–999, May 1992.

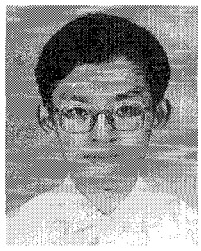

Jenn-Ming Guan was born in Taipei, Taiwan, on October 17, 1967. He received the B.S. degree in electrical engineering from National Tsinghua University, Hsinchu, Taiwan, in 1989, and the M.S. degree in electrical engineering from National Taiwan University, Taipei, Taiwan, in 1991.

Since 1991 he has been working toward the Ph.D. degree in the Department of Electrical Engineering at National Tsinghua University. His research interests include the numerical techniques for the waveguide, cavity, and dielectric resonator problems.

Ching-Chuan Su (M'87) was born in Taiwan, on October 2, 1955. He received the B.S., M.S., and Ph.D. degrees in electrical engineering from National Taiwan University in 1978, 1980, and 1985, respectively.

From 1980 to 1982, he was employed at the Industrial Technology Research Institute, Hsinchu, Taiwan, where he was responsible for the development of several IC fabrication processes for MOS products. In 1985 he joined the faculty of National Tsinghua University, Hsinchu, Taiwan, where he is an associate professor of electrical engineering. His research areas include electromagnetic theory, numerical solutions in scattering, waveguide, resonator, and MOS circuit, and fabrication of ferroelectric memory IC.